Design optimization of coreless stator axial flux-switching motor

Hossein Asgharpour-Alamdari[1], *
1, * Department of Electrical Engineering, Technical and Vocational University (TVU), Tehran, Iran
E-mail: asgharpour.alamdari@gmail.com & asgharpour_alamdari@tvu.ac.ir
Tel:+981132312902 Mobile:+989111159474 Postal Address:4714944884

Abstract: This study aimed to provide the analytical design, optimization, and three-dimensional (3D) simulation through Finite Element Method (FEM) of a coreless stator axial field flux-switching motor (AFFSM). The motor consists of two indented rotors with a coreless stator between them consisting of a magnet and winding. First of the motor electrical and magnetic design was performed and its basic parameters were calculated. Then, the optimization of the machine was evaluated implementing the Taguchi algorithm in order to minimize the motor cogging torque. Some of the basic motor dimensions, such as the magnet length and width, the rotor tooth width and height, and the back iron thickness, were selected as optimization variables, and the best combination of these variables was obtained by changing them in a certain range to achieve the desired objective. Then, the accuracy of analytical design and optimization was evaluated through forming a 3D FEM of the motor and investigating its performance. Comparison of the optimized and primary motor revealed that the optimal design had a better performance than the initial. Finally, a prototype of the proposed motor was fabricated and tested, which indicated that the experimental results were largely similar to the analytical results.

Keywords: Finite Element Method; Axial field flux-switching permanent magnet motor; Coreless; Optimization; Taguchi method;

1 Introduction

Considering the power density, higher efficiency and also the rotor losses being low, axial flux permanent magnet machines (AFPMMs) show a great advantage over the traditional radial flux permanent magnet machines (RFPMMs) [1]. The AFPMMs can be divided into two major categories; internal rotor axial flux PM machines and internal stator axial flux PM machines. In internal rotor AFPMMs the single rotor is between two stators; on the other hand in internal stator AFPMMs the single stator is between two rotors. More developments have been conducted on the internal stator axial flux PM machines for high performance applications. The yokeless and segmented armature (YASA) AFPMMs, amongst the internal stator AFPMMs are distinct for their design; this unique design separates them for their modular stator topology and also demonstrates a better performance as a result of short end windings, a higher fill factor and the absence of stator core [2], [3].

As it was mentioned before, there are many advantages to AFPMMs compared to RFPMMs. Furthermore, considering the high torque density and also the structure of axial flux machines being more compact [4] & [5], the AFPMMs are better suited for applications with high space limitations and also their applications include wind turbine

applications [6], flywheel energy storage systems, electric vehicle (EV) and also hybrid vehicles [7].

Recently, a lot of attention has been paid to the axial field flux-switching permanent magnet (AFFSPM) machines. The AFFSPM machines combine the advantages of the AFPMMs and also flux-switching machines [8], presenting a machine with a short axial length which makes it compact and robust and also presents a high power density on top of other advantages [9], [10].

As it was previously mentioned in AFPMMs with coreless stator topologies, losing the stator removes the iron losses, which eventually adds to its advantages. Additionally, removing the stator core losses leads to a higher efficiency in coreless stator AFPMMs, hence, a smaller motor stack is obtained. Also, without the stator core in these machines, the reluctance variation is eliminated that yields to the abolition of cogging torque. On the other hand, with the absence of stator core the AFPM machine needs to use more permanent magnets to compensate for the core to produce the same magnetic flux density in the air gap.

The Taguchi method is an optimization method which was initially developed by Dr. Genichi Taguchi in 40s at the Japanese Electrical Communications Laboratories. The motivation to develop this optimization method came when he realized that by using judicious planning, the cost of development can be reduced drastically [11].

In literature, the Taguchi method has been applied to various types of electrical machines such as brushless DC PM motors [12], [13], PM Synchronous Machines [14], [15], line-start PMSM [16] , induction machine [17], Reluctance Synchronous Machines or Switch Reluctance Machines [18], [19] axial flux PM Synchronous Machines [20] , linear or tubular type machines [21], [22] , and superconducting wind generator [23].

The novel AFPMM discussed in this paper is shown in the figure 1. As it can be seen the stator of this motor is coreless and consists of coil and permanent magnet. Due to interaction between permanent magnet and rotor teeth there is cogging torque where influence on proper performance of the motor. So, the goal of this paper is to reduce cogging torque with Taguchi method.

The paper is structured as follows:

Section 2 shows axial field flux-switching permanent magnet motor characteristics and design process. In section 3 machine optimization and simulation are investigated using the Taguchi method and transient magnetic time-stepping FEM. Section 4 includes the experimental results. The conclusions are included in Section 5.

2 Sizing equations

Figures 1 and 2 depict the coreless stator flux-switching motor structure proposed in this paper. With respect to this figure, stator is coreless and consists of 12 non-overlapping coils with rectangular magnets placed in them. Furthermore, two rotors with 14 teeth are in top and bottom of the stator. At any given time, some rotor tooth is placed in front of the stator permanent magnets with opposite magnetization direction as shown in Fig 3, and thus the coil flux linkage is switched and voltage is induced in each coil. The proposed motor specifications are listed in Table I.

Fig.1 Proposed AFSPMM

Table 1 Proposed motor characteristics

Fig. 2 Rotor, stator and coil

Fig. 3 Permanent magnets and rotor position

Design of the AFFSPM motor is very similar to the coreless stator and double-rotor AFPM machines [24], [25]. In the conventional coreless stator AFPM machines, the magnets are placed on the rotor and the stator coils are located between the two rotor cores. In the structure proposed in this article, the rotor consists of tooth instead of PM and the coil and magnets were in the stator, and the magnet was surrounded by the coil. In conventional axial flux motors, outer diameter calculated form (1). Where αp, Ac, kw, ws, Bmg, η, $cos(\varphi)$ and λ are the ratio of magnet width to pole pitch, electrical loading, winding factor and for the coreless stator AFPM is equal to 0.955 [23], rated speed (rpm), maximum air gap flux density (T), Efficiency, power factor and the motor inner to outer diameter ratio, respectively. Number of turns per phase and the maximum magnetic flux per pole are defined by (2) and (3) [26]. where Ef is the rms of no-load Back-EMF (V), f is the frequency (Hz), Nc is the number of coil turn and $\phi_{\max}$ (Wb) is the maximum magnetic flux per pole [27]. Frequency of the Back-EMF calculated from (4) where Nr is the number of rotor tooth and W_s is the rotor speed in rpm.

$$D_{out} = \sqrt[3]{\frac{32P_{out}}{\pi^3 \alpha_p A_c K_w w_s B_{mg}(1-\lambda^2)(1+\lambda)\cos(\varphi)}} \tag{1}$$

$$N_c = \frac{E_f}{\pi\sqrt{2} f K_w \varphi_{max}} \tag{2}$$

$$\phi_{\max} = B_{mg} A_p = B_{mg} \alpha_p \frac{\pi}{8N_r}(1-\lambda^2) D_{out}^2 \tag{3}$$

$$f = \frac{N_r w_s}{60} \tag{4}$$

3 Optimization and FEM analysis

3.1 Optimization

Cogging torque generally occurs due to the difference between the magnetic reluctance at the permanent magnet in the stator and at the rotor tooth. Presence of cogging torque in PM machines leads to the noise and vibration; hence, it is necessary to reduce it as much as possible at the design stage. So, the goal of the optimization is to reduce the peak

of cogging torque in AFFSPM motor. The cogging torque is reduced based on the assumption that the optimized motor torque is not less than the initial motor torque.

Fig. 4 Taguchi method process

Flowchart of the Taguchi method steps is demonstrated in the Figure 4. According to this figure, first of all the objective of optimization is determined. Then, the optimization variables are selected and the level of their changes is identified. Next, according to the variables and the number of levels of their changes, the Taguchi experiments table is plotted and the results of each experiment are extracted using the FEM.
After completing the simulations, the maximum cogging torque and torque are calculated for each experiment and the most suitable combination is selected according to the results.

3.1.1 Determine the optimization variables

Parameters of optimization are defined as variables *A, B, C, D* and *E*, and each parameter take 5 factor levels. *A* is the width of PM (M_w). *B* is the height of the PM (M_h). *C* is the height of rotor tooth (T_h). D is the Rotor tooth width (T_w) and *E* is the Rotor back iron height (B_i) (Figure 3). Optimization variables and they levels are illustrated in Table 2.

Table 2 Motor characteristics

3.1.2 Design and solve the orthogonal matrix of Taguchi experiment

Based on the five variables selected for optimization which are shown in Table 2 and also the five-level factor ranges, for each of the variables, the matrix of Taguchi experiments can be shown in Table 3. If the traditional optimization experiments were to be done the number of experiments would be 5^5=3125, however by using Taguchi optimization method the number of experiment required are 5×5=25 experiments.

3.1.3 Analysis of Mean Value

To statistically analyse the results of the experiments, at first the average is analysed. Taguchi optimization method uses this statically mean, which is made by orthogonal arrays and also according to Table 3 analysis results of the FEM. Equation (5) shows the average calculation formula and the results are shown in Table 4.

$$M = \frac{1}{n}\sum_{i=1}^{n} S_i \tag{5}$$

Table 3 Experimental arrays and results of FEM

Table 4 Average value of all experiments

The average of each factor level is evaluated from (6).

$$b_{xi} = \frac{1}{5}(b_x(j) + b_x(l) + b_x(m) + b_x(k) + b_x(p)) \tag{6}$$

Where b_{xi} define the average value of the factor x on the level of i_{th}. b_x shows the index of target performance under some experiment of the parameter *x* and parameters *j, k, m, l, p*

are experimental numbers. For example, the average value of peak cogging torque of factor D at level 2 is calculated as:

$$b_{D2} = \frac{1}{5}(b_D(2) + b_D(10) + b_D(13) + b_D(16) + b_D(24)) \quad (7)$$

Similarly, for all variable levels, their average can be calculated. Table 5 demonstrates the results of the analysis. Figures (5) and (6) also are a depiction of results.

Table 5 Experimental arrays and results of FEM

Fig. 5 Main factor effects on motor cogging torque

Fig. 6 Main factor effects on motor average torque

3.1.4 Analysis the impact proportion of optimization variables on the optimization

Based on the analysis results so far, to assess the relatively important design variables, and also find the best combination of them, as it can be seen in (8), analysis of variance (ANOVA) is implemented. The x in equation (8) denotes different variables which here are (*A, B, C, D* and *E*), i is the levels of those variables including: 1, 2, 3, 4 and 5 levels, P is the motor performance, Maximum cogging torque ($T_{cogging}$ (N.m)), Average Torque (Torque (N.m)), the performance average value is $L_{x_i}(P_j)$ which is shown in Table 4 and the performance average value under each level of factor variable is $L_{x_i}(P_{x_i})$ and it is shown in Table 5 and Table 6 represents the sum of squares (SS) and the proportion results.

$$SS = 5\sum_{i=1}^{5}\sum_{j=1}^{2}[L_{(x_i)}(P_{(x_i)}) - L_{(x_i)}(P_j)]^2 \quad (8)$$

Table 6 Proportion of influences produced by various factors on motor performance

3.1.5 RSM to determine the optimal combination of variables

As mentioned earlier, the aim of optimization is to minimize $T_{cogging}$, and maximize $Torque$. The response surface methodology (RSM) has been used to attain the best combination of factors. The interactions of factors with specific responses are also investigated. In an optimization study, factors are variables that are chosen to identify the best combination of them. Furthermore, responses represent key indicators that are affected by chosen factors. RSM creates a set of experiments or simulation runs to assess

responses based on the factors chosen. The following equation is a general second-order model for RSM:

$$y = c_0 + \sum_{i=1}^{n_f} c_i f_i + \sum_{i=1}^{n_f} c_{ii} f_i^2 + \sum_{i<j=2} \sum^{n_f} c_{ij} f_i f_j \quad (9)$$

Where y represents the considered response, f is selected factor, n_f is number of factors and, c's are unknown coefficients, which are obtained using regression analysis. This research aims to optimize two responses at the same time. A technique known as the desirability function is used to optimize more than one response, simultaneously. As the desirability function approaches one, the response meets the optimal solution.

As previously shown in Table 2, five independent variables are chosen to be the optimization factors. For the selected factors, RSM suggests 32 simulation runs via the approach of central composite design. Finally, RSM calculations are performed in MINITAB software, and the mathematical model to estimate the behavior of each response has been found. The designed experiments and performed simulation runs are reported in Table 7. Moreover, the result of second-order model for $T_{cogging}$ and $Torque$ are presented in equation (10) and (11).

$$\begin{aligned} T_{cogging} = {} & 53.5 + 0.538A - 2.94B - 0.183C - 3.612D - 4.47E \\ & - 0.0290A \times A - 0.0173B \times B - 0.0058C \times C + 0.0672D \times D \\ & + 0.0331E \times E - 0.0093A \times B - 0.0011A \times C + 0.0185A \times D \\ & + 0.0279A \times E + 0.0583B \times C + 0.0443B \times D + 0.2416B \times E \\ & - 0.0058C \times D + 0.0034C \times E + 0.1196D \times E \end{aligned} \quad (10)$$

$$\begin{aligned} Torque = {} & -31.0 + 0.58A + 2.25B + 1.95C + 0.90D + 0.50E \\ & + 0.0001A \times A - 0.109B \times B + 0.0143C \times C + 0.0066D \times D \\ & + 0.113E \times E + 0.0516A \times B - 0.0164A \times C - 0.0071A \times D \\ & - 0.0474A \times E - 0.0487B \times C - 0.0536B \times D - 0.018B \times E \\ & - 0.0305C \times D - 0.1216C \times E - 0.0145D \times E \end{aligned} \quad (11)$$

Using the RSM model and desirability functions, the optimal combination of factors reflecting the optimal solution is found and given in Table 8. The optimal suggestion has composite desirability of 0.967.

Table 9 also detailed the anticipated values of each response as well as the confirmation run used to calculate the RSM error. As shown, with the optimal combination reported in Table 8, i.e., A=20, B=5.13, C=14.5, D=13.64, and E=11, RSM predicts the response value of $T_{cogging}$ and Torque to be 0.65 N.m and 5.67 N.m, respectively. The confirmation run for the optimal combination has been carried out and results show that $T_{cogging}$ and Torque are 0.7 N.m and 5.5 N.m. As Table 9 depicts, the error of RSM prediction is less than 5%. Therefore, it can be concluded that RSM is trustworthy for this optimization

problem. Furthermore, as presented in Table 9, the desirability values for $T_{cogging}$ and Torque are 0.939 and 0.996, respectively, which is close to the ideal condition.

Table 7 designed experiments using RSM and performed simulation runs

Table 8 Optimal combination of factors

Table 9 Response values attained for the optimal condition

3.2 FEM analysis of initial and optimized motor

In the previous section, the desired motor optimization was investigated and the best combination was selected to achieve the desired goal. In this section, to compare the performance of the primary and optimal motor, three-dimensional analysis by the FEM is investigated. According to the variables considered in the optimization section and the results of the optimization, the specifications of the primary and optimal motors are given in Table 10. According to this table, a three-dimensional view of the primary and optimized motors is shown in Figure (7a) and Figure (7b), respectively. By comparing the dimensions of the magnet in both the initial and optimal designs, it is observed that the volume of the permanent magnets of the optimal topology is about 11% less than the primary topology.

The magnetic flux density and the flux path in the primary and optimized motor at rated current and speed are shown in Figure 8. Maximum flux densities are almost 1.2 T in the yoke and teeth. The cogging torque in the primary and final motor is shown in Figure 9. As it can be seen, the cogging torque in optimized design is about 41% less than the primary design.

Figure 10 demonstrates the motor three phase voltage in the no-load state at the rated speed. According to this figure, the peak voltage of the primary design and final design are about 86 and 92 volts, respectively, with a 6 volts difference.

Table 10 Specifications of Motors

Fig. 7 Initial and optimized motor a) Initial b) Optimized

In addition, Figure 11 shows the torque of the primary and optimal design at the rated speed. According to Figure 11, the torque curve of the optimal design has lower ripple compare to the original design due to the reduction of cogging torque.

Fig. 8 Flux density and flux path of two motors (a) Flux density in optimized motor (b) Flux density in primary motor (c) Flux path in optimized motor (d) Flux path in primary motor

Fig. 9 Cogging torque

Fig. 10 Three-Phase Back EMF at Rated Speed

Fig. 11 Torque at rated current and rated speed

4 Experimental results

In order to evaluate the accuracy of analytical analysis of the previous sections, a prototype machine is built according to the results shown in section 3. The final assembled motor is shown in Figure 12. No load Test setup was built to measure characteristics of proposed motor. Cogging torque and Back-EMF test are main parameters that measured in no load test. The test setup of the measurement of the cogging torque and no-load phase voltage are shown in Fig. 13 (a) and Fig. 13 (b), respectively. The method used to measure cogging torque is discussed in [28]. The stator was fixed to the jaws of a lathe machine and rotor rotate in low speed. In this situation a balanced beam was attached to the shaft and it was connected to the digital weight gauge. The torque is obtained from the reading of digital weight gauge. According to the Figure 13b, in the Back-EMF test, the motor shaft is connected to the lathe machine on both sides and the motor windings are connected to the oscilloscope. In this case, motor windings are open circuit; therefore, the oscilloscope indicates the resulting voltage of Back-EMF. The no-load voltage measured and calculated through the FEM and cogging torque is shown in Figure 14 and Figure15 respectively. Comparison of the obtained results and FEM results shows that the no-load voltage and cogging torque are highly similar.

Fig. 12 Assembled motor

Fig. 13 Schematic of the No load test setups a) Cogging torque test setup b) Back-EMF test setup

Fig. 14. Phase voltage of AFSPMM, simulation and experimental results

Fig. 15 Cogging torque of AFSPMM, simulation and experimental results

5 Conclusion

This study aimed to provide the analytical design, optimization, and simulation of a new AFFSPM motor with coreless stator and double rotor through FEM, and its construction. First, the motor was designed considering the rated values, and some dimensional and

electrical characteristics of the motor were extracted. Then, the designed motor was optimized using the Taguchi algorithm aiming to minimize the cogging torque. The 3D FEM model of optimized model simulated and compared to the initial motor and performance parameters such as the air gap flux density, torque, and Back-EMF, were compared. The optimization results showed that the optimized motor had a lower cogging torque, a higher torque, and a higher Back-EMF value compared to the primary structure. Finally, the motor was constructed and tested; the obtained results were then compared with those calculated in the simulation section, indicating that the experimental results were largely consistent with the analytical results.

Reference

[1] Jilong, Z., Xiaowei, Q., Xiangdong, S., et al. "Design of a Novel Axial Flux Rotor Consequent-Pole Permanent Magnet Machine," *IEEE Trans. Appl. Supercond.*, vol. 30, no. 4, pp. 1–6, 2020.

[2] Jian, L., Yang. L., Yun-Hyun, Cho., et al. "Design, Analysis, and Prototyping of a Water-Cooled Axial-Flux Permanent-Magnet Machine for Large-Power Direct-Driven Applications," *IEEE Trans. Ind. Appl.*, vol. 55, no. 4, pp. 3555–3565, 2019.

[3] Youhua, W., Jiawei, L., Chengcheng, L., et al. "Development of a high-performance axial flux PM machine with SMC cores for electric vehicle application," *IEEE Trans. Magn.*, vol. 55, no. 7, pp. 1–4, 2019.

[4] Jilong, Z., Xiaowei, Q., and Mingyao, L., "Model Predictive Torque Control of a Hybrid Excited Axial Field Flux-Switching Permanent Magnet Machine," *IEEE Access*, vol. 8, pp. 33703–33712, 2020.

[5] Wei, Z., Zexian, Y., Liangguan, Z., et al. "Speed Sensorless Control of Hybrid Excitation Axial Field Flux-Switching Permanent-Magnet Machine Based on Model Reference Adaptive System," *IEEE Access*, vol. 8, pp. 22013–22024, 2020.

[6] Kostas, L., Alexandros, M., Ilias, K., et al. "Acoustic Noise of Axial Flux Permanent Magnet Generators in Locally Manufactured Small Wind Turbines," *IET Renew. Power Gener.*, vol. 13, no. 15, pp. 2922–2928, 2019.

[7] Nasrudin, A.R., Hew Wooi, P., and Mohammad Faridun Naim, T. "Design of an in-wheel axial flux brushless DC motor for electric vehicle," in *2006 International Forum on Strategic Technology*, 2006, pp. 16–19.

[8] Wasiq, U., Faisal, K., Erwan, S., et al. "Torque characteristics of high torque density partitioned PM consequent pole flux switching machines with flux barriers," *CES Trans. Electr. Mach. Syst.*, vol. 4, no. 2, pp. 130–141, 2020.

[9] Ju Hyung, K., Yingjie, L., and Bulent, S., "Sizing, Analysis, and Verification of Axial Flux-Switching Permanent Magnet Machine," *IEEE Trans. Ind. Appl.*, vol. 55, no. 4, pp. 3512–3521, 2019.

[10] Ju Hyung, K., Yingjie, L., Emrah, C., et al. "Influence of Rotor Tooth Shaping on Cogging Torque of Axial Flux-Switching Permanent Magnet Machine," *IEEE Trans. Ind. Appl.*, vol. 55, no. 2, pp. 1290–1298, 2018.

[11] Ranjit K, R., *A primer on the Taguchi method*. Society of Manufacturing Engineers, 2010.

[12] Chang-Chou, H., San-Shan, H., Cheng-Tsung, L., et al. "Optimal design of a high speed SPM motor for machine tool applications," *IEEE Trans. Magn.*, vol. 50, no. 1, pp. 1–4, 2013.

[13] Teck-Seng, L., Shixin, C., and Xianke, G. "Robust torque optimization for BLDC spindle motors," *IEEE Trans. Ind. Electron.*, vol. 48, no. 3, pp. 656–663, 2001.

[14] Huimin, W., Shu, L., Shuang, W., et al. "Optimal Design of Permanent Magnet Structure to Reduce Unbalanced Magnetic Pull in Surface-Mounted Permanent-Magnet Motors," *IEEE Access*, vol. 8, pp. 77811–77819, 2020.

[15] Sujin, L., Kyuseob, K., Sugil, C., et al. “Optimal design of interior permanent magnet synchronous motor considering the manufacturing tolerances using Taguchi robust design,” *IET Electr. Power Appl.*, vol. 8, no. 1, pp. 23–28, 2014.

[16] Albert Johan, S., Rong-Jie, W., and Andries J, G. “Multiobjective design of a line-start PM motor using the Taguchi method,” *IEEE Trans. Ind. Appl.*, vol. 54, no. 5, pp. 4167–4176, 2018.

[17] Yen-Shin, L., Juo-Chiun, L., and Jennshing Jersey, W. “Direct torque control induction motor drives with self-commissioning based on Taguchi methodology,” *IEEE Trans. Power Electron.*, vol. 15, no. 6, pp. 1065–1071, 2000.

[18] Wenju, Y., Hao, C., Xuekun, L., et al. “Design and multi-objective optimisation of switched reluctance machine with iron loss,” *IET Electr. Power Appl.*, vol. 13, no. 4, pp. 435–444, 2019.

[19] Ji, Z., Li, H., Chen. Z., et al. “Design and Optimization of Permanent Magnet Assisted Synchronous Reluctance Motor for Better Torque Performance,” in *2019 22nd International Conference on Electrical Machines and Systems (ICEMS)*, 2019, pp. 1–4.

[20] Wenshuai, Z., Xuzhen. H., and Tianpeng. J. “Design of Tubular Permanent Magnet Synchronous Linear Motor in a Wide Temperature Range Environment by Taguchi-fuzzy Method,” in *2019 22nd International Conference on Electrical Machines and Systems (ICEMS)*, 2019, pp. 1–5.

[21] Juncai, S., Fei, D., Jiwen, Z., et al. “Optimal design of permanent magnet linear synchronous motors based on Taguchi method,” *IET Electr. Power Appl.*, vol. 11, no. 1, pp. 41–48, 2017.

[22] Hyung Jin, S., Rod, B., Zhongyi, G., et al. “Design of a 12-MW HTS wind power generator including a flux pump exciter,” *IEEE Trans. Appl. Supercond.*, vol. 26, no. 3, pp. 1–5, 2016.

[23] Surong, H., Jian, L., Franco, L., et al. “A comparison of power density for axial flux machines based on general purpose sizing equations,” *IEEE Trans. energy Convers.*, vol. 14, no. 2, pp. 185–192, 1999.

[24] Jacek F, G., Rong-Jie, W., and Maarten J, K. “*Axial flux permanent magnet brushless machines*,” Springer Science & Business Media, 2008.

[25] Maarten J, K., Rong-Jie, W., and Francois G. R. “Analysis and performance evaluation of axial flux air-cored stator permanent magnet machine with concentrated coils,” in *2007 IEEE International Electric Machines & Drives Conference*, 2007, vol. 1, pp. 13–20.

[26] Kostas, L., Katerina, T., Thomas. P., et al. “Design of axial flux permanent magnet generators using various magnetic materials in locally manufactured small wind turbines,” in *2016 XXII International Conference on Electrical Machines (ICEM)*, 2016, pp. 1545–1551.

[27] Maarten J, K., Rong-Jie, W., and Francois G. R. “Analysis and performance of axial flux permanent-magnet machine with air-cored nonoverlapping concentrated stator windings,” *IEEE Trans. Ind. Appl.*, vol. 44, no. 5, pp. 1495–1504, 2008.

[28] Z. Q. Z. “A simple method for measuring cogging torque in permanent magnet machines,” in 2009 IEEE Power & Energy Society General Meeting, 2009, pp. 1–4.

Hossein Asgharpour-Alamdari received the Ph.D. from Semnan University, Iran, in 2017. He is currently an Assistant Professor with Technical and Vocational University (TVU), Babol branch, Iran. His research interests are power system stability and control, power system protection, electrical machines and their application in renewable energy.

Figure captions

Fig.1 Proposed AFSPMM

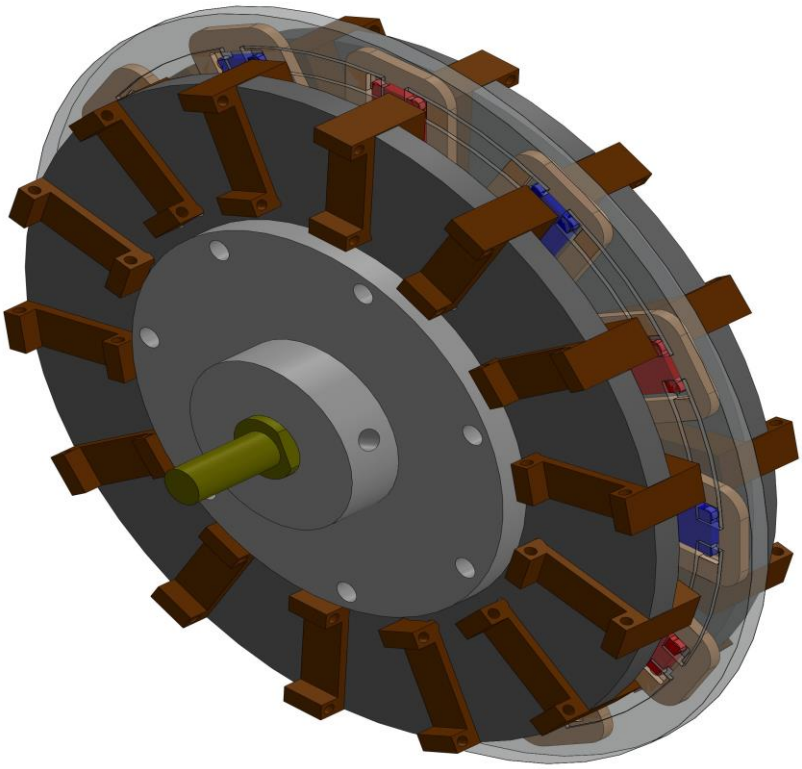

Fig. 2 Rotor, stator and coil

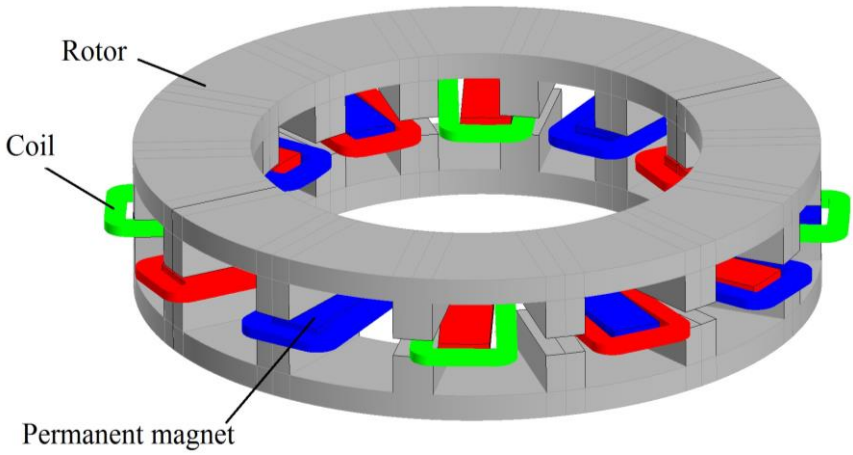

Fig. 3 Permanent magnets and rotor position

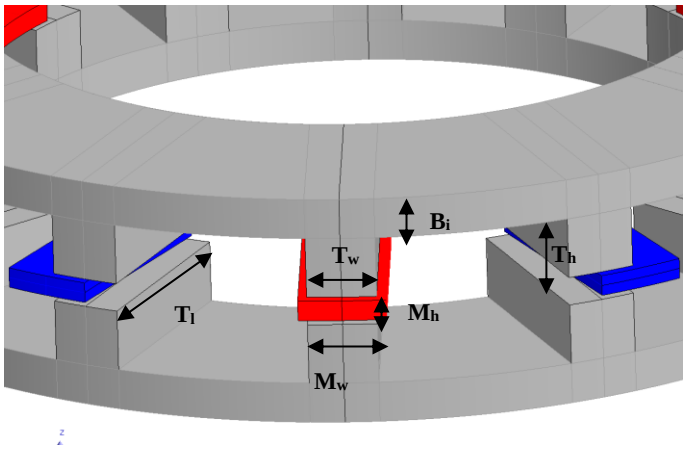

Fig. 4 Taguchi method process

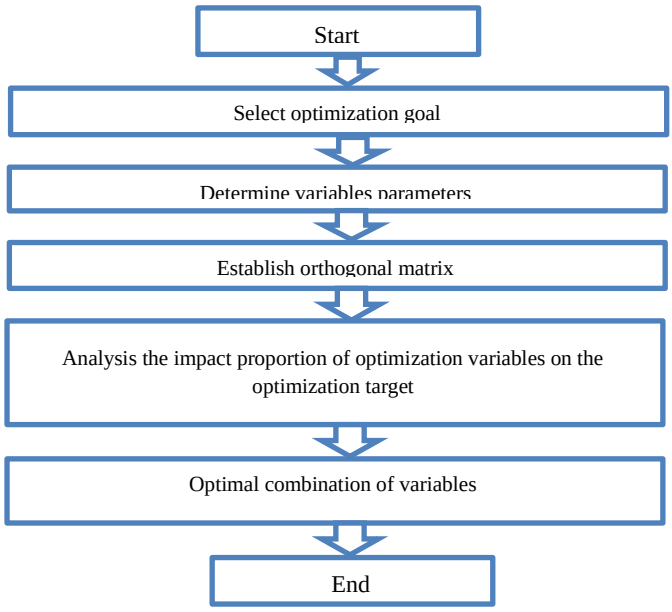

Fig. 5 Main factor effects on motor cogging torque

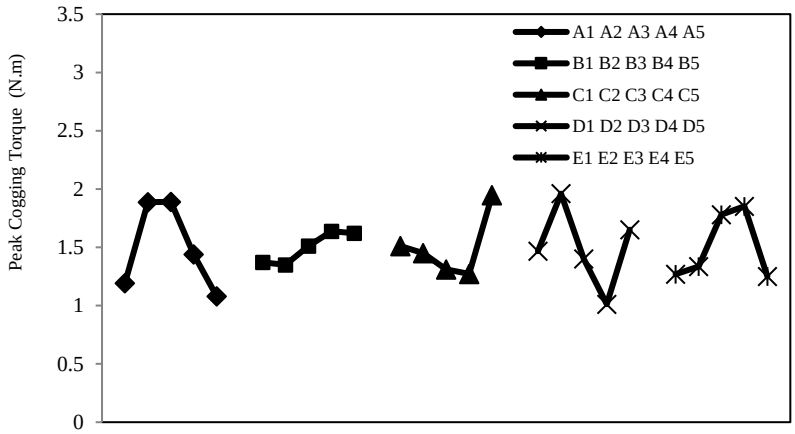

Fig. 6 Main factor effects on motor average torque

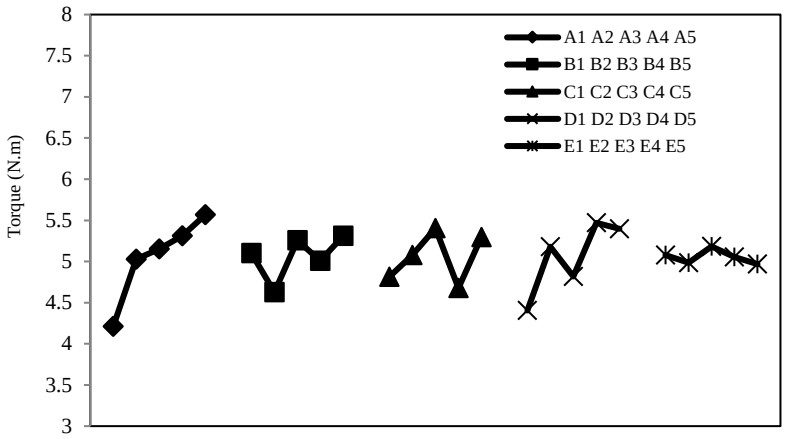

Fig. 7 Initial and optimized motor a) Initial b) Optimized

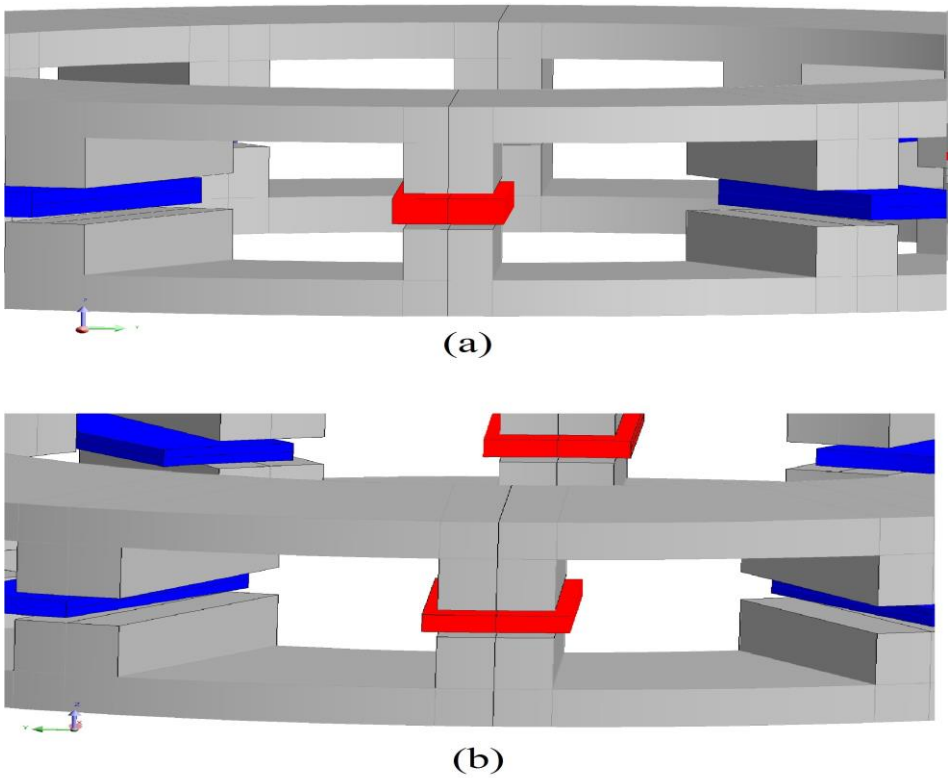

Fig. 8 Flux density and flux path of two motors (a) Flux density in optimized motor (b) Flux density in primary motor (c) Flux path in optimized motor (d) Flux path in primary motor

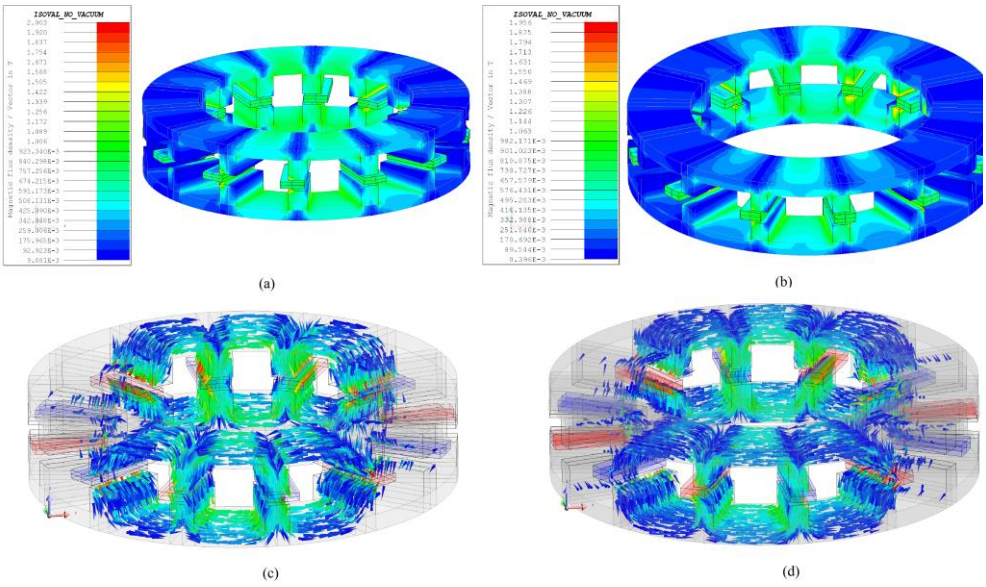

Fig. 9 Cogging torque

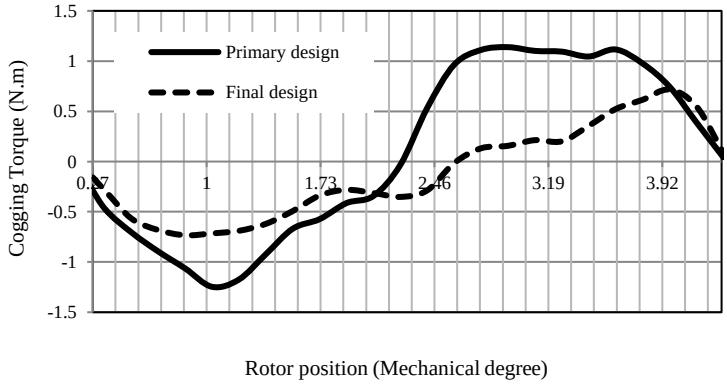

Fig. 10 Three-Phase Back EMF at Rated Speed

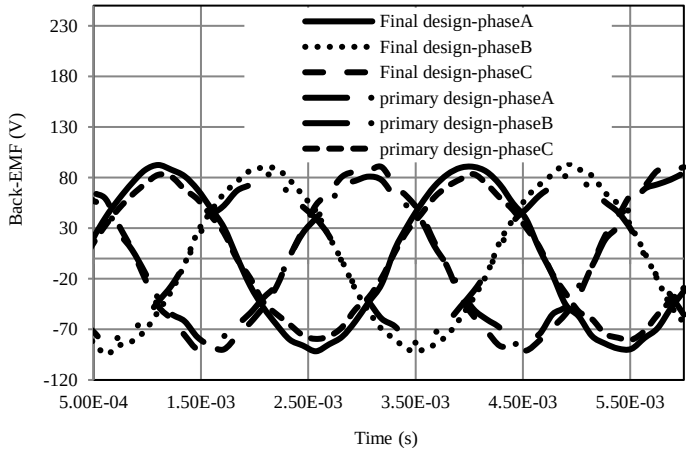

Fig. 11 Torque at rated current and rated speed

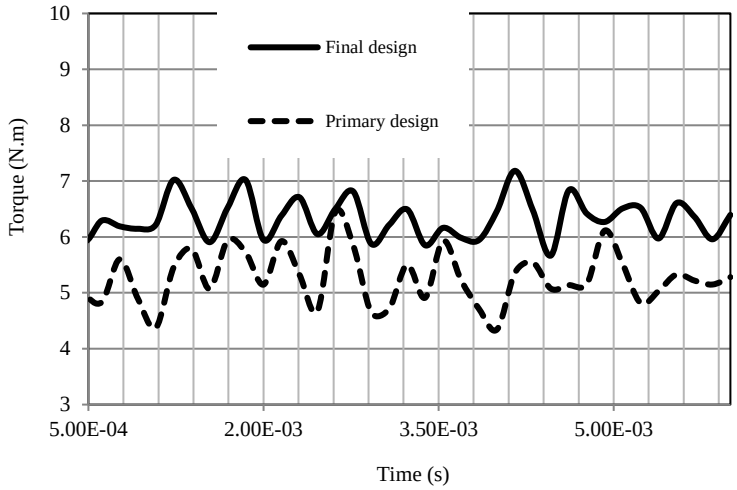

Fig. 12 Assembled motor

Fig. 13 Schematic of the No load test setups a) Cogging torque test setup b) Back-EMF test setup

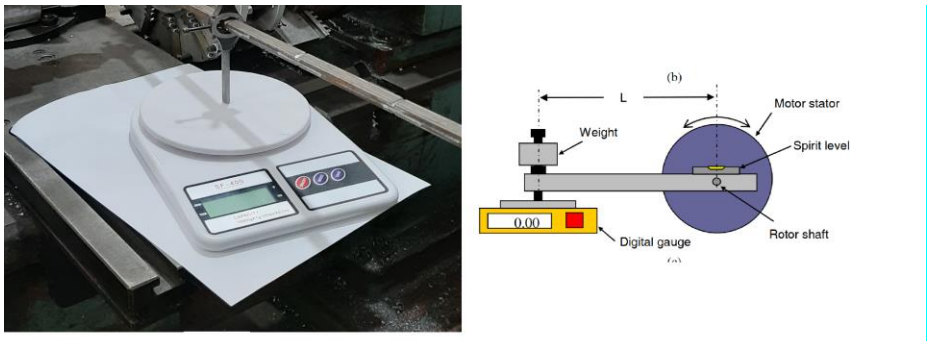

(a)

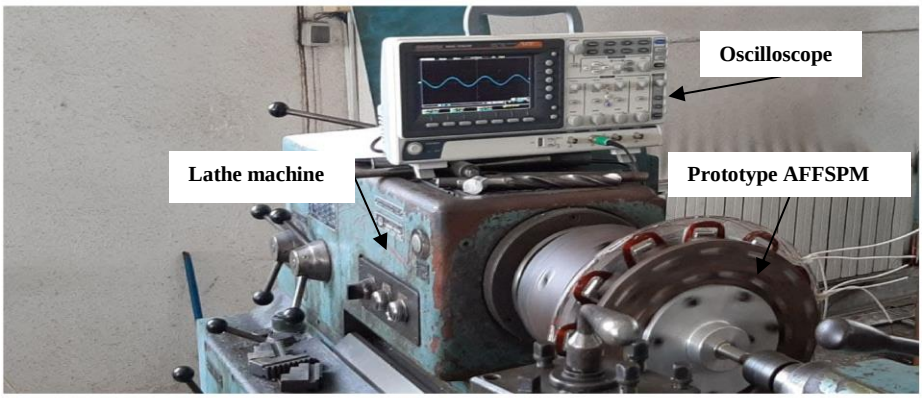

(b)

Fig. 14. Phase voltage of AFFSPM motor, simulation and experimental results

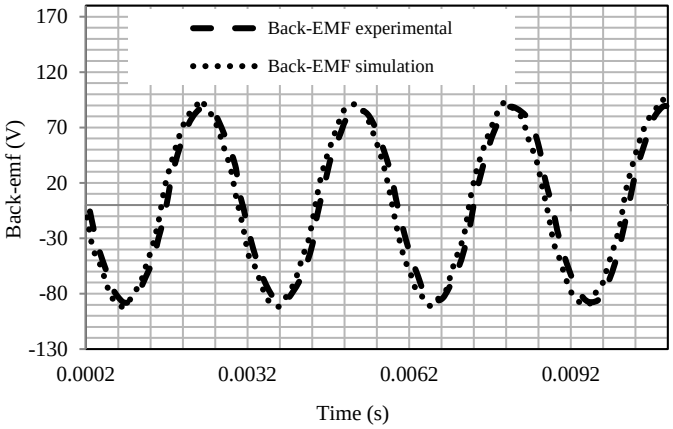

Fig. 15 Cogging torque of AFFSPM motor, simulation and experimental results

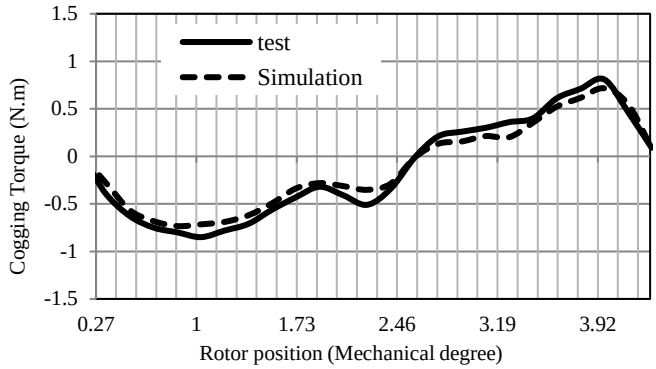

Table captions

Table 1 Proposed motor characteristics

Output power	Number of stator magnets	Number of rotor pole pairs	Rated speed	Rated frequency
1000 W	12	14	1500 RPM	350 HZ

Table 2 Motor characteristics

Variables	**Level 1**	**Level 2**	**Level 3**	**Level 4**	**Level 5**	**initial**
A (M_w)	12	14	16	18	20	16
B (M_h)	5	6	7	8	9	7
C (T_h)	7	9	11	13	15	13
D (T_w)	10	12	14	16	18	12
E (B_i)	7	8	9	10	11	10

Table 3 Experimental arrays and results of FEM

Experiment	***A***	***B***	***C***	***D***	***E***	***$T_{cogging}$ (N.m)***	***Torque (N.m)***
1	1	1	1	1	1	1.15	3.25
2	1	2	2	2	2	1	3.85
3	1	3	3	3	3	1.1	4.915
4	1	4	4	4	4	1.21	4.05
5	1	5	5	5	5	1.5	4.8
6	2	1	2	3	4	1.8	4.56
7	2	2	3	4	5	1.15	5.32
8	2	3	4	5	1	1.3	5.21
9	2	4	5	1	2	2.18	4.76
10	2	5	1	2	3	3	5.2885
11	3	1	3	5	2	1.8	5.4845
12	3	2	4	1	3	1.6	3.71

Experiment	*A*	*B*	*C*	*D*	*E*	$T_{cogging}$ *(N.m)*	*Torque (N.m)*
13	3	3	5	2	4	3.5	5.76
14	3	4	1	3	5	1.4	4.5255
15	3	5	2	4	1	1.15	6.28
16	4	1	4	2	5	1.2	5.09
17	4	2	5	3	1	1.65	4.76
18	4	3	1	4	2	0.65	5.5
19	4	4	2	5	3	2.3	5.8
20	4	5	3	1	4	1.4	5.4
21	5	1	5	4	3	0.9	6.2
22	5	2	1	5	4	1.35	5.5
23	5	3	2	1	5	1	4.905
24	5	4	3	2	1	1.1	5.9
25	5	5	4	3	2	1.05	5.33

Table 4 Average value of all experiments

Parameter	**$T_{cogging}$ (N.m)**	**Torque (N.m)**
Average value	1.599	5

Table 5 Experimental arrays and results of FEM

Variables	**Level of each factor**	**$T_{cogging}$ (N.m)**	**Torque (N.m)**
A	1	1.252	4.213
	2	1.886	5.0277
	3	1.93	5.152
	4	1.44	5.31
	5	1.08	5.567
B	1	1.37	5.1
	2	1.35	4.628
	3	1.51	5.258
	4	1.678	5.0071
	5	1.68	5.3125
C	1	1.55	4.8128
	2	1.45	5.079
	3	1.31	5.4039
	4	1.272	4.678
	5	2.006	5.296
D	1	1.466	4.405
	2	1.96	5.1777
	3	1.44	4.8181
	4	1.012	5.47
	5	1.71	5.3989
E	1	1.27	5.08
	2	1.336	4.9849
	3	1.78	5.1827
	4	1.852	5.054
	5	1.25	4.9681

Table 6 Proportion of influences produced by various factors on motor performance

Variables	$T_{cogging}$ (N.m)		Torque (N.m)	
	SS	**Proportion (%)**	**SS**	**Proportion (%)**
A	1.046	41.27	0.6958	34.64
B	0.29	11.6	0.0443	2.21
C	0.381	15.03	0.2803	13.95
D	0.7841	30.94	0.5944	29.59
E	0.0293	1.16	0.3939	19.61
Total	**2.54**	**100**	**2**	**100**

Table 7 designed experiments using RSM and performed simulation runs

Run number	Factors (variables)					Responses (objectives)	
	A (M_w)	B (M_h)	C (T_h)	D (T_w)	E (B_i)	$T_{cogging}$ (N.m)	Torque (N.m)
1	16	7	11	14	9	1.2	5
2	16	7	11	14	9	1.2	5
3	16	7	11	14	9	1.2	5
4	14	8	13	16	8	0.818	5.4
5	14	6	13	16	10	0.441	5.29
6	14	6	13	12	8	1.89	5.015
7	18	8	9	12	10	1.33	5.89
8	18	8	13	16	10	2.19	5.5759
9	16	7	11	14	9	0.91	4.9975
10	16	7	11	14	9	0.91	4.9975
11	14	8	13	12	10	1.82	4.7517
12	14	8	9	16	10	1.1571	5.485
13	14	6	9	16	8	0.41	4.93
14	16	7	11	18	9	2	5.93
15	18	6	9	16	10	0.88	6
16	18	8	9	16	8	0.52	6.3186
17	16	7	7	14	9	1.46	4.45
18	16	5	11	14	9	1.233	4.95
19	18	8	13	12	8	1.8	6.295
20	16	7	11	10	9	2.54	5.2
21	16	7	11	14	11	1.1	6.75
22	18	6	13	16	8	0.8	6.35
23	14	8	9	12	8	1.22	4.25
24	16	7	11	14	7	1.556	5.07275
25	16	9	11	14	9	1.02	5.1
26	18	6	13	12	10	1.118	5.08
27	18	6	9	12	8	1.745	4.757
28	20	7	11	14	9	0.77	6.6721
29	16	7	15	14	9	0.747	6.9265
30	16	7	11	14	9	0.874	6.778
31	12	7	11	14	9	0.694	4.25
32	14	6	9	12	10	0.68	4.41

Table 8 Optimal combination of factors

Factors	Optimum value
A (M_w)	20
B (M_h)	5.13
C (T_h)	14.5
D (T_w)	15.64
E (B_i)	11

Table 9 Response values attained for the optimal condition

Response	Optimum results by RSM	Confirmation run	Error (%)	desirability
$T_{cogging}$ (N.m)	0.67	0.7	4.28	0.939
Torque (N.m)	5.67	5.5	3.09	0.996

Table 10 Specifications of Motors

Parameter	unit	Primary	optimized
Rated power (P_{out})	W	1000	1000
Rated speed (w_s)	rpm	1500	1500
Number of phase (m)	-	3	3
Number of stator coils (Q_c)	-	12	12
Number of rotor tooth (N_r)	-	28	28
Rotor outer diameter (D_{out})	mm	270	270
Air gap Length (g)	mm	1.5	1.5
Ratio of inner to outer diameter (λ)	-	0.6	0.6
Magnet height (M_h)	mm	7	5.13
Magnet width (M_w)	mm	16	20
Number of turns per phase (N_{phase})	-	260	260
Magnet length (M_L)	mm	50	50
Tooth width (T_w)	mm	14	15.64
Tooth height (T_h)	mm	13	14.5
Tooth length (T_L)	mm	50	50
Back iron (Bi)	-	8	11
Magnet type	-	Neodymium Iron Boron: 42/15	Neodymium Iron Boron: 42/15